# Cross-Examination of Ultrafast Structural, Interfacial, and Carrier $Dynamics \ of \ Supported \ Monolayer \ MoS_2$

Xing He,† Mazhar Chebl,† Ding-Shyue Yang\*

Department of Chemistry, University of Houston, Houston, Texas 77204 United States

<sup>&</sup>lt;sup>†</sup>These authors contributed equally to this work.

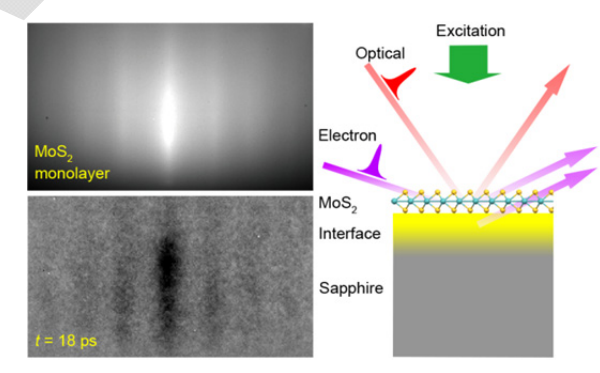
<sup>\*</sup>To whom correspondence should be addressed. Email: yang@uh.edu

#### Abstract

In this report, the ultrafast structural, interfacial, and carrier dynamics of monolayer  $MoS_2$  supported on sapphire are cross-examined by the combination of ultrafast electron diffraction (UED) and transient reflectivity techniques. The out-of-plane motions directly probed by reflection UED suggest a limited anisotropy in the atomic motions of monolayer  $MoS_2$ , which is distinct from that of related materials such as graphene and  $WSe_2$ . Besides thermal diffusion, the  $MoS_2$ -sapphire interface exhibits structural dynamics trailing those of the overlaying  $MoS_2$  and are in stark contrast with the sapphire bulk, which is consistent with the limited thermal boundary conductance. These structural dynamics provide justification for the determination of carriers being trapped by defects in  $\sim 600$  femtoseconds and releasing energy within few picoseconds. The rich findings attest the strength of combining techniques with real-time optical and direct structure probes for detailed understanding of dynamical processes in functional materials.

**Keywords**: supported two-dimensional materials, 2D, transition metal dichalcogenides, femtosecond spectroscopy, lattice dynamics, van der Waals

## **TOC Graphic**



Since the experimental discovery of graphene, research of the properties and applications of single- and few-layer 2-dimensional (2D) materials and van der Waals solids has been growing exponentially in recent years.<sup>1, 2</sup> Transition metal dichalcogenides (TMDs), in particular, have attracted great attention because of their versatile structures and tunable optical and electronic properties, besides the typical benefits of 2D materials with good mechanical strength and flexibility as well as large electrical and thermal conductivity.<sup>3, 4</sup> Molybdenum disulfide (MoS<sub>2</sub>) is a prototypical example, which exhibits major changes in its electronic structure especially for the evolution from an indirect bandgap of 1.3 eV for the bulk to a direct gap of 1.9 eV for a monolayer.<sup>5</sup> Such an electronic modification results in layer-dependent efficiencies in photo- and electroluminescence,<sup>5-7</sup> which opens up various potential (opto)electronic applications such as light-emitting diodes, solar cells, and field-effect transistors. Opportunities may also exist when large external stimuli or fields are applied.<sup>8</sup> To further understand light-matter interactions in 2D and related materials at the fundamental level, studies of ultrafast electronic and structural dynamics following photoexcitation at different levels are therefore needed.

Previously, studies using time-resolved all-optical spectroscopy have suggested a few relaxation mechanisms for carriers photogenerated in monolayer MoS<sub>2</sub> (1L-MoS<sub>2</sub>), including exciton–exciton annihilation below the Mott density,<sup>9, 10</sup> defect-assisted electron–hole recombination,<sup>11</sup> and carrier–phonon scattering.<sup>12, 13</sup> Measurements of photoluminescence produced from radiative recombination of carriers have often been considered as one of the methods to characterize 1L-MoS<sub>2</sub>, with influence from the formation of excitons and trions,<sup>14-16</sup> a supporting dielectric medium,<sup>17, 18</sup> applied strain,<sup>19, 20</sup> temperature,<sup>12</sup> and surface treatment.<sup>6</sup> In these studies, the photoinjection levels were in the range of 4×10<sup>9</sup> to 8×10<sup>12</sup> cm<sup>-2</sup> to avoid complex mechanisms that may occur at higher carrier densities. In contrast, only a few reports

exist to date about photoinduced structural dynamics of 1L-MoS<sub>2</sub> or TMDs. Ultrafast electron diffraction (UED) in a transmission geometry has been used to examine 1L-MoS<sub>2</sub> transferred onto a copper TEM grid with an amorphous carbon layer, showing in-plane atomic displacements and the inference of induced out-of-plane rippling, at the injection level of ~5×10<sup>14</sup> cm<sup>-2</sup>. Early-time structural dynamics of monolayer and bilayer MoSe<sub>2</sub> probed by transmission UED at ~10<sup>14</sup> cm<sup>-2</sup> suggest a softening of vibrational modes in the excited state for efficient and rapid energy transfer between the electronic and the lattice subsystems. Ultrafast x-ray diffraction in a reflection geometry has been used to investigate the anisotropic in-plane and out-of-plane lattice vibrations of WSe<sub>2</sub> supported on sapphire, within a rather small temporal window of 10 picoseconds (ps). <sup>23</sup>

A few fundamental issues of 1L-MoS<sub>2</sub> have not been examined in detail. For example, graphene has been found to have different in-plane and out-of-plane atomic motions<sup>24, 25</sup> and Debye temperatures<sup>26, 27</sup> and WSe<sub>2</sub> exhibits prominent anisotropy in lattice vibrations at early times following photoexcitation.<sup>23</sup> The degree of anisotropy of 1L-MoS<sub>2</sub> remains unknown because of the lack of direct probing of out-of-plane dynamics for comparison. Furthermore, structural dynamics at the interface between 2D materials and their supporting substrates have not been resolved to date, whose understanding is relevant to actual devices in that solid supports will likely be present for most applications instead of free-standing films, and an underlying substrate may influence the behavior of supported TMDs.<sup>17, 18</sup> In addition, time-resolved dynamics of photogenerated carriers at higher injection levels require further study, whose results should be consistent with the subsequent lattice dynamics probed by structure-specific methods.

In this report, structural, interfacial, and carrier dynamics of sapphire-supported 1L-MoS<sub>2</sub>

are cross-examined using the combination of UED and transient reflectivity measurements, at elevated injection densities ranging from 5.80×10<sup>12</sup> to 1.13×10<sup>14</sup> cm<sup>-2</sup>. We note our capability to probe the out-of-plane lattice motions and to differentiate the dynamics of the MoS<sub>2</sub>-sapphire interfacial structure because of the small penetration depth of 30-keV electrons incident in a reflection geometry. It is found that out-of-plane lattice motions of supported 1L-MoS<sub>2</sub> are comparable to the in-plane counterparts reported earlier in a transmission study<sup>21</sup> and hence a single Debye temperature can be assigned for both in-plane and out-of-plane dimensions. Thermal diffusion via the interface governs the recovery at longer times whereby the thermal boundary conductance is determined. More significantly, diffractions produced by the MoS<sub>2</sub>-sapphire interface exhibit time-dependent changes trailing those of the 2D material itself, which implies the different behavior of the interfacial structure compared to that of the sapphire bulk. These structural dynamics provide information for a consistent analysis of the results of optical pump-probe measurements, where the trapping of the photogenerated carriers by defects is found in ~600 femtoseconds (fs).

Structural dynamics of monolayer MoS<sub>2</sub>. Shown in Figure 1a is the diffraction pattern of 1L-MoS<sub>2</sub> acquired at an incidence angle of  $\theta_{\rm in}$  = 3.8° without photoexcitation. The observation of multiple diffraction streaks at all grazing incidence and azimuthal rotational angles confirms the 2D nature of the monolayer, which was grown by chemical vapor deposition (CVD) with azimuthally rotated crystallites. The diffraction streaks (ensemble-probed from an area of  $15\times230~\mu\text{m}^2$ ) are well indexed with a hexagonal lattice and a lattice constant of 3.18 Å is obtained.<sup>28</sup> At incidence angles higher than 4.6°, the more apparent diffraction spots and Kikuchi lines indicate the probing of the interfacial structure and the surface region of the supporting

substrate underneath the 2D material due to increased electron penetration.

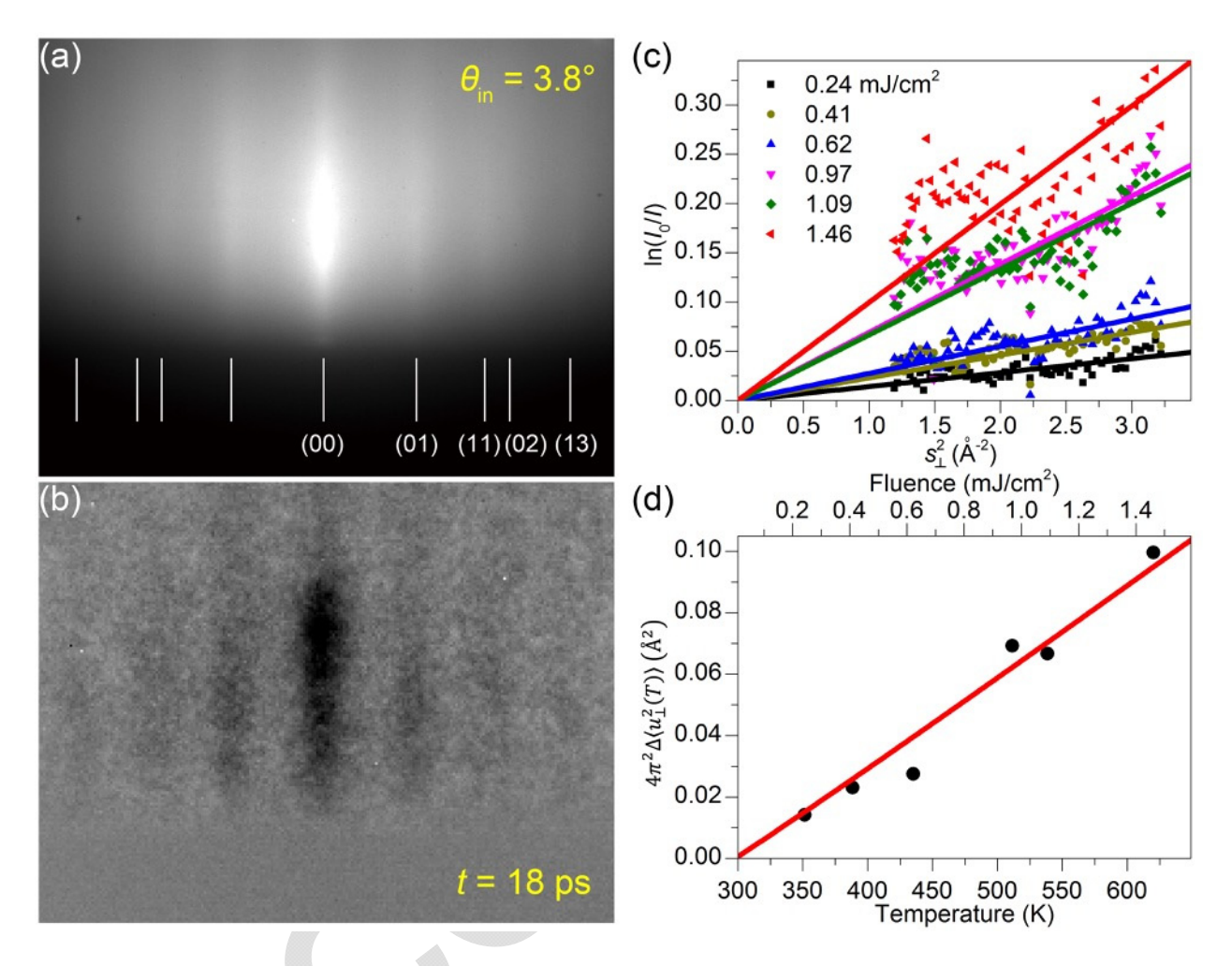


Figure 1. Electron diffraction and photoinduced changes of 1L-MoS<sub>2</sub>. (a) Diffraction of 1L-MoS<sub>2</sub> acquired at an incidence angle of  $\theta_{\rm in} = 3.8^{\circ}$  without laser excitation. The 2D Miller indices are given. (b) Diffraction difference image at t = 18 ps referenced to (a). (c) Diffraction intensity changes along the center streak as a function of  $s_{\perp}^2$  at different laser fluences used. The symbols are the experimental results obtained via intensity curve fits, and the lines are linear fits according to Equation 1. (d) Mean-square atomic displacement increments as a function of the maximum temperature reached at the respective apparent fluence. The line is a fit by Equation 3.

Following an above-gap excitation by 515-nm photons, the intensity of 1L-MoS<sub>2</sub> diffractions decrease within 20 ps (Figure 1b). It is crucial to first confirm that the observed diffraction changes originate from structural motions, not from any surface-related field or Coulombic effects. Shown in Figure 2b is the lack of any intensity changes near the shadow edge, which signifies the absence of significant surface electric fields that could alter the paths of grazing electron scattering (see also Supplementary Information and Figure S2). Given that no apparent structural transition exists at the temperature and excitation fluences used, the Debye–Waller effect describing the relation between diffraction intensity and the increased motions of ions in 1L-MoS<sub>2</sub> is considered:<sup>29</sup>

$$\ln\left(\frac{I_0}{I(t)}\right) = 2W(t) = \Delta \left\langle \left(\vec{q} \cdot \vec{u}(t)\right)^2 \right\rangle = 4\pi^2 s_\perp^2 \cdot \Delta \langle u_\perp^2(t) \rangle \tag{1}$$

where the  $I_0$  and I(t) are, respectively, the diffraction intensities of the center diffraction streak before the zero of time and at time t after excitation, W the Debye-Waller factor,  $\vec{u}$  the atomic displacement vector,  $\vec{q} = 2\pi \vec{s}_{\perp}$  the scattering vector of the center diffraction streak, and  $s_{\perp} = 2\sin(\theta/2)/\lambda$  the vertical momentum transfer perpendicular to the scattering surface, with  $\theta$  being the total scattering angle and  $\lambda = 0.0698$  Å the de Broglie wavelength of 30-keV electrons. Thus, according to Equation 1,  $\ln(I_0/I)$  is directly proportional to  $s_{\perp}^2$  at a given time and fluence that correspond to a certain increment value of the out-of-plane mean-square displacement,  $\Delta\langle u_1^2(t)\rangle$ .

This is indeed our observation, which validates the use of reflection UED to probe transient out-of-plane lattice motions. A linear relation is observed between  $\ln(I_0/I)$  and  $s_{\perp}^2$  for all laser fluences used (Figure 1c). Furthermore, the consistence with the Debye-Waller effect signifies the thermalization of random atomic motions in 1L-MoS<sub>2</sub> at early times. It is found that the absorption of 44  $\mu$ J/cm<sup>2</sup> (3% of the apparent fluence of 1.46 mJ/cm<sup>2</sup> at 515 nm) leads to

 $\Delta\langle u_{\perp}^2(t)\rangle \cong 2.5 \times 10^{-3} \,\text{Å}^2$ ; in the earlier transmission UED study, the absorption of 220  $\mu\text{J/cm}^2$  (6.6% of the apparent fluence of 3.3 mJ/cm<sup>2</sup> at 400 nm) yields in-plane  $\Delta\langle u_{\parallel}^2(t)\rangle \cong 1.25 \times 10^{-2} \,\text{Å}^2.^{21}$  Thus, the excellent proportionality between the absorbed energy densities and the induced in-plane and out-of-plane mean-square displacement increments, indicates that the thermalized atomic motions after several ps are essentially isotropic, showing limited anisotropy unlike those of graphene and WSe<sub>2</sub>. This shows that dynamical behaviors of different 2D materials vary significantly even though they share the 2D structural motif.

The temperature dependence of mean-square atomic displacements is given by<sup>29</sup>

$$\langle u_{\perp}^{2}(T)\rangle + 2\langle u_{\parallel}^{2}(T)\rangle \cong 3\langle u_{\perp}^{2}(T)\rangle = \frac{9\hbar^{2}}{\bar{m}k_{B}\Theta_{D}} \left[ \frac{1}{4} + \left( \frac{T}{\Theta_{D}} \right)^{2} \int_{0}^{\frac{\Theta_{D}}{T}} \frac{xdx}{e^{x} - 1} \right]$$
(2)

where  $u_{\parallel}(T)$  is the one-dimensional in-plane atomic displacement component,  $\hbar$  the reduced Planck constant,  $\overline{m}$  the average atomic mass,  $k_B$  the Boltzmann constant,  $\Theta_D$  the Debye temperature, and  $x = \hbar \omega / k_B T$  with  $\omega$  being the phonon frequency. The first equal sign is valid here because 1L-MoS<sub>2</sub> exhibits effectively isotropic atomic motions. Hence, the experimentally-obtained out-of-plane mean-square atomic displacement has the following temperature dependence:

$$4\pi^2 \Delta \langle u_{\perp}^2(T) \rangle = \frac{3h^2}{\bar{m}k_B \Theta_D} \left[ \left( \frac{T}{\Theta_D} \right)^2 \int_0^{\frac{\Theta_D}{T}} \frac{x dx}{e^x - 1} - \left( \frac{T_0}{\Theta_D} \right)^2 \int_0^{\frac{\Theta_D}{T_0}} \frac{x dx}{e^x - 1} \right] \cong \frac{3h^2(T - T_0)}{\bar{m}k_B \Theta_D^2} \quad \text{when } T \gtrsim \Theta_D \quad (3)$$

where  $T_0 = 297$  K is the initial temperature and the maximum T for each fluence is determined with the specific heat of C = 0.397 J/g·K, the density of  $\rho = 5.00$  g/cm<sup>3</sup>, and a thickness of d = 0.72 nm for 1L-MoS<sub>2</sub>,<sup>30</sup> considering that a thermal equilibrium is reached after several ps (see below). A fit of the fluence-dependent results in Figure 1d yields  $\Theta_D = 580$  K, which agrees well with the theoretical values for both monolayer and bulk MoS<sub>2</sub> at room temperature<sup>31, 32</sup> and the value reported by the transmission UED study for in-plane motions.<sup>21</sup>

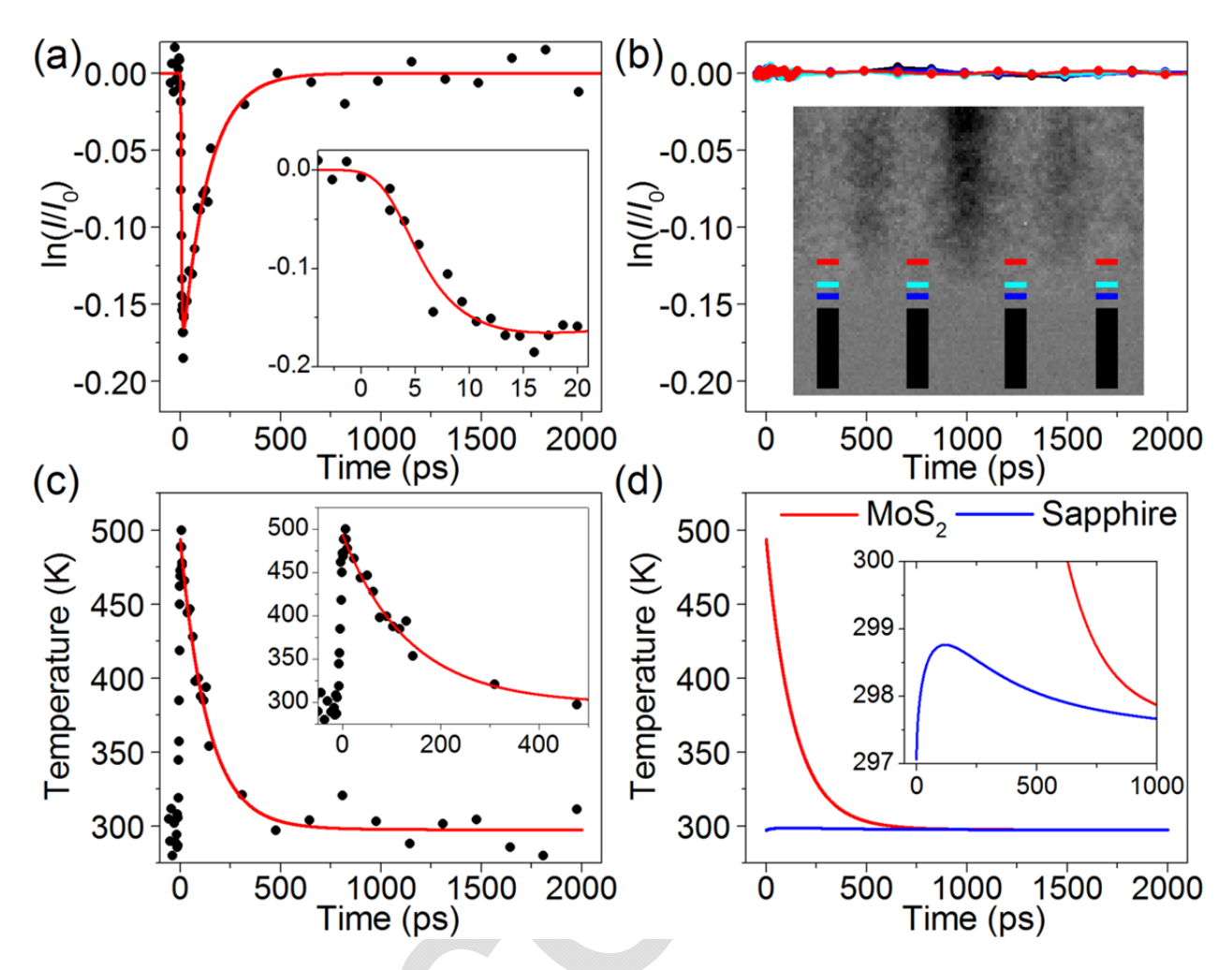


**Figure 2.** Time dependence of structural changes of 1L-MoS<sub>2</sub> at 0.97 mJ/cm<sup>2</sup>. (a) Diffraction intensity change as a function of the delay time. The solid line is a fit according to Equation 4. The inset shows the early-time dynamics. (b) Absence of intensity changes in the shadow edge region between the diffraction streaks (selected regions of interest are color-coded in the diffraction). (c) Effective temperature derived from the UED data (dots). The solid line gives the simulation result of one-dimensional thermal diffusion. The inset shows the dynamics within 500 ps. (d) Numerically simulated temperatures of MoS<sub>2</sub> and sapphire as a function of the delay time.

With regard to the temporal dependence, the diffraction intensity dynamics are fitted to the following function,

$$\ln[I(t)/I_0] = A \cdot \left(1 - e^{-t/\tau_r}\right) \cdot e^{-t/\tau_d} \tag{4}$$

where A < 0 is a proportional constant and  $\tau_r$  and  $\tau_d$  are the time constants for the rise and recovery of the observed changes, respectively. A Gaussian function with a full width of ~2.5 ps at half-maximum is used for convolution to account for the instrumental response time (mostly contributed by the velocity mismatch between the optical excitation and the grazing electron probe pulses). A good fit is obtained, with  $\tau_r = 4.0 \pm 2.6$  ps and  $\tau_d = 140 \pm 20$  ps (Figure 2a). It is noted that the value of  $\tau_r$  agrees with the typical time for carrier–phonon and phonon–phonon scattering processes at elevated injection densities. In fact, this is the time scale ( $\tau_r \sim 4$  ps for the out-of-plane motions following the time constant of ~2 ps obtained for the in-plane motions<sup>21</sup>) for phonons to thermalize and establish an effective temperature, which is consistent with the use of the Debye–Waller factor after the first 10 ps for the structural dynamics of 1L-MoS<sub>2</sub>. In what follows the recovery part of the dynamics is shown to originate from heat diffusion with a single time constant of  $\tau_d$ , thus further provides a consistent picture for thermal energy transport via the interface.

Heat diffusion via the interface. From the diffraction intensity change, a temperature can be assigned at each delay time after 10 ps using Equations 1 and 3 (Figure 2c). A set of equations considering one-dimensional heat transfer from 1L-MoS<sub>2</sub> to the unexcited supporting sapphire substrate are used in the numerical simulation for time dependence (see Supporting Information for details).<sup>33</sup> It becomes clear that the temperature of 1L-MoS<sub>2</sub> should essentially follows a first-order ordinary differential equation (Equation S1) because of the large temperature difference between 1L-MoS<sub>2</sub> and sapphire, which results from the relatively slow heat transfer across the interface and the good thermal conductivity of sapphire limiting its temperature increase (Figure

2d). Thus, the single exponential decay function in Equation 4 is justified, with  $\tau_d^{-1} \cong \sigma/(C\rho d)$  where  $\sigma$  is the thermal boundary conductance of MoS<sub>2</sub> monolayer on sapphire. It is determined to be 10 MW m<sup>-2</sup> K<sup>-1</sup>, which is similar to the values of 15 MW m<sup>-2</sup> K<sup>-1</sup> for MoS<sub>2</sub> on amorphous carbon<sup>21</sup> and below 20 MW m<sup>-2</sup> K<sup>-1</sup> on a few solid substrates.<sup>34</sup>

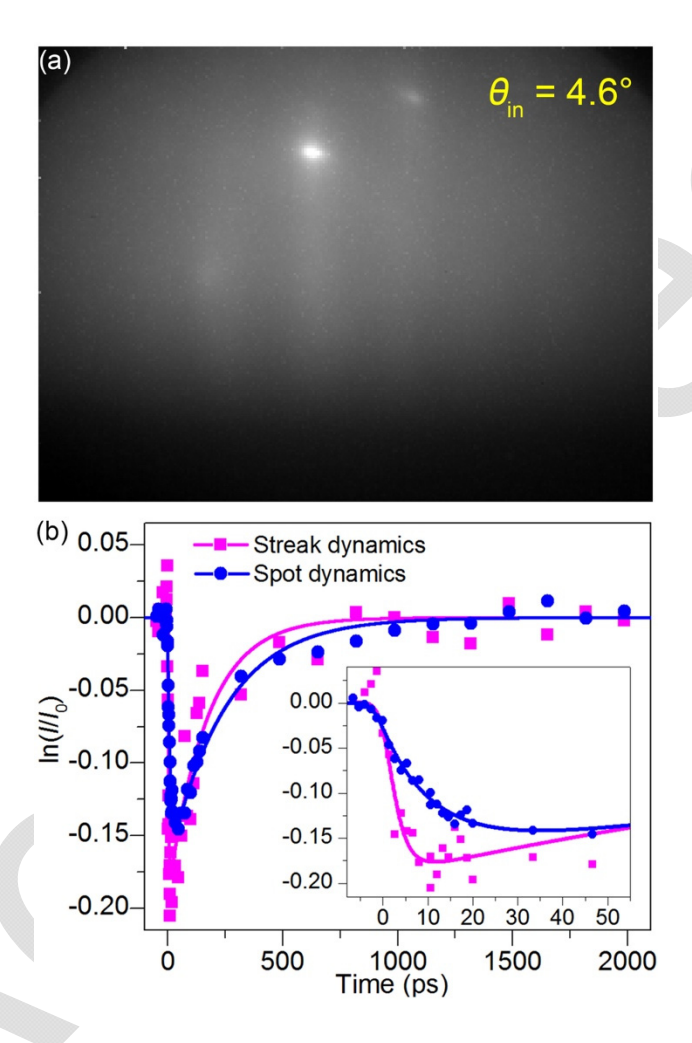


Figure 3. Structural dynamics of the  $MoS_2$ -sapphire interface. (a) Electron diffraction image acquired at a high incidence angle of 4.6°, showing weaker streaks from 1L- $MoS_2$  and a few distinguished spots originated from the interface. (b) Intensity changes of the center diffraction streak and spot as a function of time at 0.97 mJ/cm<sup>2</sup>. The solid curves are fits to Equation 4 convoluted with a Gaussian instrumental response function. The inset shows the early-time dynamics, where the change of the diffraction spot trailing that of the streak is evident.

Structural dynamics at the interface. Further details are found in the structural dynamics at the MoS<sub>2</sub>-sapphire interface beyond the aforementioned thermal diffusion model. At a higher incidence angle of  $\theta_{in} = 4.6^{\circ}$ , electrons are able to probe the interfacial region beneath the 2D layer because of the increased penetration depth. (The elastic mean free path of 30-keV electrons in MoS<sub>2</sub> is calculated to be ~108 Å using the elastic scattering cross sections of Mo and S, which leads to a probe depth of  $\sim 7.2$  Å at  $\theta_{\rm in} = 3.8^{\circ}$  essentially the same as the 2D layer thickness.) Therefore, the observed diffraction spots on the streaks in Figure 3a are mainly contributed by the top layers of the sapphire substrate with modulation by 1L-MoS<sub>2</sub>, which is consistent with simulated diffraction patterns using the kinematic scattering theory. Here, both the interfacial region of sapphire and the diffraction modulation by the 2D material are essential for the following reasons. First, without the overlaying MoS<sub>2</sub>, no time-dependent changes are observed from sapphire diffraction spots given that no excitation is made to sapphire by 515-nm photons (Figure S3); hence, its temperature increase as a result of thermal diffusion should be small (Figure 2d, inset). Second, the limited penetration of 30-keV electrons at  $\theta_{\rm in}$  = 4.6° signifies the probing of only the interfacial layers of sapphire, whose behavior can be different from that of the bulk.35 We note that effects from a transient surface electric field as a possible cause for our observation can be confidently ruled out, as has been shown earlier in the discussion of the structural dynamics of MoS<sub>2</sub>.

Shown in Figure 3b are the time-dependent intensity changes of both the center diffraction streak and spot. It is evident that the dynamics of the latter trail those of the former. A fit of the streak data to Equation 4, which represent the structural dynamics of the overlaying 1L-MoS<sub>2</sub>, gives  $\tau_r = 2.5$  ps and  $\tau_d = 170$  ps, whose values are consistent with those derived from Figure 2a even though the noise level is higher here because of the low intensity at  $\theta_{\rm in} = 4.6^{\circ}$ . In

contrast, the diffraction spot intensity change exhibits the time constants of  $\tau'_r = 12$  ps and  $\tau'_d = 240$  ps. The prominent increase in  $\tau'_r$  compared to  $\tau_r$  (with some increase in  $\tau'_d$  compared to  $\tau_d$ ) is thus in good agreement with the kinetics of the enlarged thermal motions of atoms, first initiated and thermalized in 1L-MoS<sub>2</sub> and then coupled to the interfacial layers below for relaxation. It should be noted that atoms at a materials surface experience reduced to no stress along the surface normal direction. Consequently, the atoms in the interfacial layers of sapphire exhibit motions that are greater compared to those in the bulk characterized by the small temperature increase (Figure 2d). Moreover, the large difference between  $\tau'_r$  and  $\tau_r$  is an experimental manifestation of the weak van der Waals coupling and mismatch of phonon density of states between materials, leading to the rather limited value obtained for the thermal boundary conductance.<sup>34</sup>

Once the different behavior of the interface and the substrate bulk is confirmed, the observed intensity decrease of  $\ln(I/I_0) \cong -0.15$  at 30~50 ps may be well explained (Figure 3b, inset). With the Debye temperature of MoS<sub>2</sub> (580 K) and sapphire (1042 K), a temperature increase of ~170 K and ~130 K are deduced, respectively, considering the two extreme cases that the diffraction spot is only contributed by either component. The fact that these values agree with that of the overlaying film—a temperature increase of about 135–155 K from the effective temperature of 435–455 K shown in the inset of Figure 2c—indicates a thermal exchange and equilibrium between the film and the interfacial structure, which is reasonable because of their direct contact.

Carrier dynamics. Determination of the photocarrier dynamics of a material may be better achieved with the knowledge of its structural dynamics, especially for elevated injection

densities when other processes including structural and thermo-optic components also contribute to the optical pump-probe signals. Shown in Figure 4a are the transient reflectivity changes,  $\Delta R/R$ , of sapphire-supported 1L-MoS<sub>2</sub> at room temperature following 515-nm photoexcitation, at various initial carrier densities  $N_0$  ranging from  $5.80 \times 10^{12}$  to  $8.1 \times 10^{13}$  cm<sup>-2</sup>. At each apparent

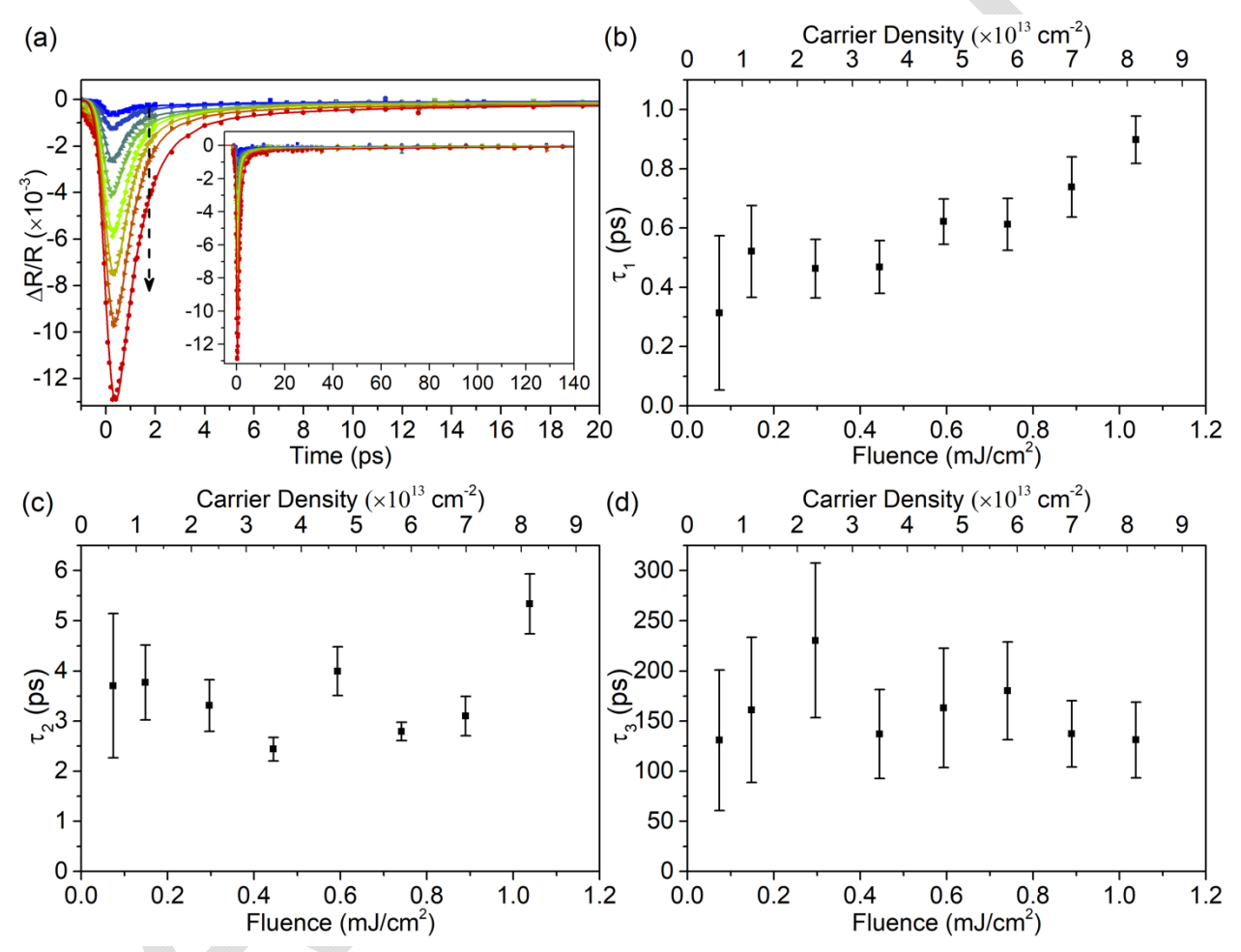


**Figure 4.** Time-dependent optical pump-probe results of supported 1L-MoS<sub>2</sub>. (a) Transient reflectivity acquired with a 1030-nm probe. The dashed arrow indicates the result of increasing the photogenerated carrier density. Dots represent the experimental data, and the solid lines are fits using the 3-exponential model described in the text. The inset shows the longer-time dynamics. (b-d) Time constants ( $\tau_1$ ,  $\tau_2$ , and  $\tau_3$ , respectively) obtained from the fits as a function of the carrier density. The error bars give the standard deviations.

laser fluence used, the reflectivity decreases to a minimum value in the instrumental response time followed by a recovery to the initial state on a ps time scale. The value of the initial decrease may be explained by the mechanisms of free-carrier absorption, band filling, and bandgap renormalization, although theoretical modifications are needed to account for the 2D material.<sup>36-39</sup>

The time-dependent recovery can be described by a 3-exponential model,  $A e^{-t/\tau_1} + B e^{-t/\tau_2} + C e^{-t/\tau_3}$  (see below for the justification) convoluted with a Gaussian instrumental response function, where  $\tau_i$ 's ( $\tau_1 < \tau_2 < \tau_3$ ) represent the time constants of three recovery processes and A, B, and C are their respective amplitudes. It is found that in the range of carrier density used, the fastest process accounts for  $\sim$ (84 ± 7)% of the recovery of the transient change on the average, whereas  $\sim$ (14 ± 6)% and  $\sim$ (2 ± 2)% are for the second and the third components, respectively (the standard deviation is indicated). In addition, the time constants obtained from the fits do not exhibit a strong dependence on laser fluence (Figure 4, b–d). The fastest component, with similar  $\tau_1 \sim$  600 fs, can be attributed to the process of carrier trapping by defects; namely, removal of the free carriers by such a mechanism effectively diminishes the transient change at early times (Figure 4b). This is consistent with previous reports for CVD-grown TMDs with a minimal dependence of the sub-ps time constant on the carrier density. <sup>11,40</sup>, <sup>41</sup> The small increase in  $\tau_1$  observed at the highest fluences used may be due to a bottleneck and/or hot-phonon effect that causes elongation of the carrier-trapping process.

It is noted that  $\tau_2 \sim 3.5$  ps and  $\tau_3 \sim 160$  ps (Figure 4, c-d) are satisfactorily consistent with the time constants ( $\tau_r$  and  $\tau_d$ ) obtained from the UED data (Figure 2a). Such an agreement allows the identification of the second and third components in the transient reflectivity results as the phonon thermalization and heat diffusion processes during the recovery, thus justifies the use

of the aforementioned 3-exponential model. These assignments could be ambiguous if only alloptical pump–probe results are available. Hence, it is crucial to conduct a cross examination of the photoinduced carrier and structural dynamics, such as presented here for sapphire-supported 1L-MoS<sub>2</sub> using the combination of optical and UED experiments. Moreover, it is concluded that the energy release from the trapped carriers to the lattice in the present fluence range must take place immediately, so to be fully consistent with the phonon thermalization process in a few ps and the success of the Debye–Waller description for the following thermal motions. Such a result also indicates a fast carrier–phonon coupling in MoS<sub>2</sub> via the emission of optical phonons in hundreds of fs, <sup>42</sup> instead of a slow process in some tens of ps. <sup>12, 13, 43</sup>

Here, we consider the possibility of a few other carrier relaxation mechanisms to explain the observed transient reflectivity and time dependence. Exciton–exciton annihilation, with a second-order rate equation, is applicable for relatively low injection levels below the Mott density of  $\sim 4.3 \times 10^{12}$  cm<sup>-2</sup> <sup>39</sup> or  $\sim 1 \times 10^{13}$  cm<sup>-2</sup>. <sup>44</sup> Auger recombination with a third-order rate equation, on the other hand, may be important at high laser fluences. For these two mechanisms, the effective rate constants should have a clear dependence on the injected carrier densities. However, they may be ruled out based on the fact that the density range used here is above the Mott density and the obtained time constant  $\tau_1$  remains similar (Figure 4b). In fact, the lack of a density dependence for  $\tau_1$  is anticipated for carrier trapping by a given density of defects. We note that depending on the preparation method for the material, the defect density may greatly differ, which may result in extended carrier lifetimes observed in a large single-crystalline specimen. <sup>39</sup> How the structural dynamics are then affected may be the subject of a further study.

Finally, we would like to address the issue of limited anisotropy in the atomic motions of MoS<sub>2</sub> compared to those of other 2D materials. Before the development of ultrafast diffraction

methods, atomic root-mean-square displacements (RMSDs) have been derived via thermal analyses of diffractions obtained in equilibrium. For graphite and WSe<sub>2</sub>, clear anisotropy in the RMSDs has been found, whose ratios between the out-of-plane and in-plane motions are about 5.5 and 4, respectively. 45, 46 For graphene, a corresponding ratio of 6.8 was obtained. 47 In contrast, the anisotropy of MoS<sub>2</sub> is largely reduced, where the out-of-plane to in-plane RSMD ratios are 1.6 and 1.3 for Mo and S, respectively.<sup>28</sup> Although insufficient to provide direct prediction of photoinduced dynamical behavior of materials, especially in monolayer cases, the diffraction results in equilibrium appear to be in line with the observations made using ultrafast techniques in terms of the degree of anisotropy in lattice motions. It is well known that for photoinjected carriers, the electron-phonon coupling in graphite and graphene is highly anisotropic, first to the in-plane strongly coupled optical phonons followed by phonon-phonon scattering to induce out-of-plane motions. 48 In the present study, 1L-MoS<sub>2</sub> is found to exhibit comparable out-of-plane and in-plane RSMDs following photoexcitation and hence limited dynamical anisotropy, which is consistent with the former x-ray diffraction results. The microscopic origins could be due to the reduction of the lattice symmetry in TMDs, which would allow additional electron-phonon coupling mechanisms<sup>49</sup> and hence reduce the degree of anisotropy compared to that of graphene. However, this structural symmetry argument may not fully explain the case of WSe<sub>2</sub>, which means that the electronic and phonon structures may also play an important role. Interestingly, the initial coupling to the out-of-plane A<sub>g</sub><sup>1</sup> mode was observed in monolayer WSe2 by optical transient transmission,50 which is opposite to the observation by femtosecond surface x-ray scattering in the first 10 ps.<sup>23</sup> This disagreement as well as the less-studied subject to date about the dynamic anisotropy in lattice motions of 2D materials suggest the need for more studies including theoretical investigations. In this regard,

reflection UED with surface specificity and an adjustable probe depth may be helpful in providing direct information about the out-of-plane motions.

In summary, the structural, interfacial, and carrier dynamics of MoS<sub>2</sub> monolayer supported on a sapphire substrate were cross-examined at the excitation levels of 5.80×10<sup>12</sup> to 1.13×10<sup>14</sup> cm<sup>-2</sup> above the Mott density threshold, using reflection UED to specifically probe the out-of-plane lattice motions and the interface as well as optical transient reflectivity for electronic and structural processes. A consistent picture was thus obtained to identify the main processes involved. At early times after the above-gap photoexcitation, the injected carriers are trapped by defects in ~600 fs, followed by the release of the carrier energy to phonons via carrier-phonon coupling within few ps. Phonon scattering and thermalization also occur on a similar time scale, resulting in atomic motions well described by the Debye-Waller factor. Surprisingly, these random atomic motions of a MoS<sub>2</sub> monolayer were found to exhibit little anisotropy, which is in stark contrast with those of other 2D materials such as graphene and WSe<sub>2</sub>. At longer times, heat diffusion across the interface for energy dissipation to the substrate takes place with a time constant of  $\sim \! 140~ps$  and a thermal boundary conductance of  $10~MW~m^{-2}$ K<sup>-1</sup>. We further observed the structural dynamics at the MoS<sub>2</sub>-sapphire interface that trails the dynamics of the overlaying 2D film and is evidently different from the nonabsorbing sapphire bulk; such a finding is unique for reflection UED and may not be easily accessed or resolved by other methods. Given the rich observations presented here, the combined use of reflection UED and transient spectroscopy to examine in detail the ultrafast dynamics of other substratesupported 2D materials and van der Waals solids is anticipated.

# **Experimental section**

Monolayer MoS<sub>2</sub> grown by the CVD method on sapphire(0001) was purchased from 2DLayer. It

was found that annealing the specimens in vacuum at an elevated temperature (above 100 °C) improved the film quality, according to the increase in the intensities of the streak-like diffractions. The monolayer was also confirmed by its prominent photoluminescence near the red end of the visible spectrum compared to that of the bulk (see Supporting Information). Throughout the measurements of the dynamics, the specimen was placed on a 5-axis high-resolution manipulator in ultra-high vacuum with a base pressure of  $\sim 2\times 10^{-10}$  torr.

Experimental details about the reflection UED and optical transient reflectivity measurements have been described previously.<sup>51, 52</sup> In short, the 515-nm, 2.41-eV photoexcitation pulses with a repetition rate of 2 kHz were produced by second harmonic generation of the fundamental output (1030 nm) of a Yb:KGW regenerative amplifier laser system. The photoexcitation beam was loosely focused on the specimen surface at a near-normal incidence angle, resulting in a footprint of ~600 µm in the full width at half-maximum (FWHM). A tiny fraction of the remaining fundamental output was used as the optical probe in transient reflectivity, incident at an angle of 35° with a probed range of ~270×220 μm² in FWHM. The electron-generating, 257-nm ultraviolet pulses were produced by another stage of second harmonic generation of the 515-nm beam. In the UED experiments, the electron probe pulses produced from a lanthanum hexaboride photocathode were accelerated to 30 keV and focused on the specimen surface for diffraction at a grazing incidence angle. Hence, the convergent electron beam had a footprint of~15×230 µm<sup>2</sup> at a grazing angle of 3.8°, which was fully enclosed within the photoexcited region. The number of photoelectrons per pulse was measured to be <250. Finally, the diffraction patterns were recorded by an imaging system composed of a phosphor screen and a gated image intensifier lens-coupled to a CMOS camera.

## ASSOCIATED CONTENT

# **Supporting Information**

Photoluminescence of MoS<sub>2</sub> monolayer and bulk, effect of surface transient electric fields on reflection UED experiments, simulation of heat diffusion via the interface, diffraction changes of bare sapphire

### **AUTHOR INFORMATION**

# **Corresponding Author**

\*Email: <u>yang@uh.edu</u> Phone: +1 713-743-6022.

## **ORCID**

Xing He: 0000-0001-5341-5662

Ding-Shyue Yang: 0000-0003-2713-9128

#### **Author Contributions**

<sup>†</sup>These authors contributed equally to this work.

#### Notes

The authors declare no competing financial interest.

# **ACKNOWLEDGMENTS**

This research was supported by a National Science Foundation CAREER Award (Grant no. CHE-1653903), the R. A. Welch Foundation (Grant no. E-1860), and the Samsung Global Research Outreach program.

#### **REFERENCE**

- Butler, S. Z.; Hollen, S. M.; Cao, L. Y.; Cui, Y.; Gupta, J. A.; Gutiérrez, H. R.; Heinz, T. F.; Hong, S. S.; Huang, J. X.; Ismach, A. F.; Johnston-Halperin, E.; Kuno, M.; Plashnitsa, V. V.; Robinson, R. D.; Ruoff, R. S.; Salahuddin, S.; Shan, J.; Shi, L.; Spencer, M. G.; Terrones, M.; Windl, W.; Goldberger, J. E. Progress, challenges, and opportunities in two-dimensional materials beyond graphene, *ACS Nano* 2013, 7, 2898-2926.
- 2. Novoselov, K. S.; Mishchenko, A.; Carvalho, A.; Castro Neto, A. H. 2D materials and van der Waals heterostructures, *Science* **2016**, 353, aac9439.
- 3. Chhowalla, M.; Shin, H. S.; Eda, G.; Li, L. J.; Loh, K. P.; Zhang, H. The chemistry of two-dimensional layered transition metal dichalcogenide nanosheets, *Nat. Chem.* **2013**, 5, 263-275.
- Jariwala, D.; Sangwan, V. K.; Lauhon, L. J.; Marks, T. J.; Hersam, M. C. Emerging device applications for semiconducting two-dimensional transition metal dichalcogenides, ACS Nano 2014, 8, 1102-1120.
- 5. Mak, K. F.; Lee, C.; Hone, J.; Shan, J.; Heinz, T. F. Atomically thin MoS<sub>2</sub>: a new direct-gap semiconductor, *Phys. Rev. Lett.* **2010**, 105, 136805.
- Amani, M.; Lien, D.-H.; Kiriya, D.; Xiao, J.; Azcatl, A.; Noh, J.; Madhvapathy, S. R.; Addou, R.; KC, S.; Dubey, M.; Cho, K.; Wallace, R. M.; Lee, S.-C.; He, J.-H.; Ager, J. W.; Zhang, X.; Yablonovitch, E.; Javey, A. Near-unity photoluminescence quantum yield in MoS<sub>2</sub>, Science 2015, 350, 1065-1068.
- 7. Li, D.; Cheng, R.; Zhou, H.; Wang, C.; Yin, A.; Chen, Y.; Weiss, N. O.; Huang, Y.; Duan, X. Electric-field-induced strong enhancement of electroluminescence in multilayer molybdenum disulfide, *Nat. Commun.* **2015**, 6, 7509.
- 8. Sun, Z.; Hasan, T.; Torrisi, F.; Popa, D.; Privitera, G.; Wang, F.; Bonaccorso, F.; Basko, D. M.; Ferrari, A. C. Graphene mode-locked ultrafast laser, *ACS Nano* **2010**, **4**, 803-810.
- Sun, D.; Rao, Y.; Reider, G. A.; Chen, G.; You, Y.; Brézin, L.; Harutyunyan, A. R.; Heinz, T. F. Observation of rapid exciton-exciton annihilation in monolayer molybdenum disulfide, *Nano Lett.* 2014, 14, 5625-5629.

- 10. Yu, Y.; Yu, Y.; Xu, C.; Barrette, A.; Gundogdu, K.; Cao, L. Fundamental limits of exciton-exciton annihilation for light emission in transition metal dichalcogenide monolayers, *Phys. Rev. B* **2016**, 93, 201111.
- 11. Wang, H.; Zhang, C.; Rana, F. Ultrafast dynamics of defect-assisted electron-hole recombination in monolayer MoS<sub>2</sub>, *Nano Lett.* **2015**, 15, 339-345.
- 12. Korn, T.; Heydrich, S.; Hirmer, M.; Schmutzler, J.; Schüller, C. Low-temperature photocarrier dynamics in monolayer MoS<sub>2</sub>, *Appl. Phys. Lett.* **2011**, 99, 102109.
- 13. Shi, H.; Yan, R.; Bertolazzi, S.; Brivio, J.; Gao, B.; Kis, A.; Jena, D.; Xing, H. G.; Huang, L. Exciton dynamics in suspended monolayer and few-layer MoS<sub>2</sub> 2D crystals, *ACS Nano* **2013**, 7, 1072-1080.
- 14. Lin, Y.; Ling, X.; Yu, L.; Huang, S.; Hsu, A. L.; Lee, Y.-H.; Kong, J.; Dresselhaus, M. S.; Palacios, T. Dielectric screening of excitons and trions in single-layer MoS<sub>2</sub>, *Nano Lett.* **2014**, 14, 5569-5576.
- Cadiz, F.; Tricard, S.; Gay, M.; Lagarde, D.; Wang, G.; Robert, C.; Renucci, P.; Urbaszek,
  B.; Marie, X. Well separated trion and neutral excitons on superacid treated MoS<sub>2</sub> monolayers, *Appl. Phys. Lett.* 2016, 108, 251106.
- 16. Christopher, J. W.; Goldberg, B. B.; Swan, A. K. Long tailed trions in monolayer MoS<sub>2</sub>: Temperature dependent asymmetry and resulting red-shift of trion photoluminescence spectra, *Sci. Rep.* **2017**, 7, 14062.
- 17. Buscema, M.; Steele, G. A.; van der Zant, H. S. J.; Castellanos-Gomez, A. The effect of the substrate on the Raman and photoluminescence emission of single-layer MoS<sub>2</sub>, *Nano Res.* **2014**, 7, 561-571.
- Atallah, T. L.; Wang, J.; Bosch, M.; Seo, D.; Burke, R. A.; Moneer, O.; Zhu, J.; Theibault, M.; Brus, L. E.; Hone, J.; Zhu, X. Y. Electrostatic screening of charged defects in monolayer MoS<sub>2</sub>, J. Phys. Chem. Lett. 2017, 8, 2148-2152.
- 19. Conley, H. J.; Wang, B.; Ziegler, J. I.; Haglund, R. F., Jr.; Pantelides, S. T.; Bolotin, K. I. Bandgap engineering of strained monolayer and bilayer MoS<sub>2</sub>, *Nano Lett.* **2013**, 13, 3626-3630.

- 20. He, K.; Poole, C.; Mak, K. F.; Shan, J. Experimental demonstration of continuous electronic structure tuning via strain in atomically thin MoS<sub>2</sub>, *Nano Lett.* **2013**, 13, 2931-2936.
- 21. Mannebach, E. M.; Li, R.; Duerloo, K. A.; Nyby, C.; Zalden, P.; Vecchione, T.; Ernst, F.; Reid, A. H.; Chase, T.; Shen, X.; Weathersby, S.; Hast, C.; Hettel, R.; Coffee, R.; Hartmann, N.; Fry, A. R.; Yu, Y.; Cao, L.; Heinz, T. F.; Reed, E. J.; Dürr, H. A.; Wang, X.; Lindenberg, A. M. Dynamic structural response and deformations of monolayer MoS<sub>2</sub> visualized by femtosecond electron diffraction, *Nano Lett.* 2015, 15, 6889-6895.
- 22. Lin, M.-F.; Kochat, V.; Krishnamoorthy, A.; Bassman, L.; Weninger, C.; Zheng, Q.; Zhang, X.; Apte, A.; Tiwary, C. S.; Shen, X.; Li, R.; Kalia, R.; Ajayan, P.; Nakano, A.; Vashishta, P.; Shimojo, F.; Wang, X.; Fritz, D. M.; Bergmann, U. Ultrafast non-radiative dynamics of atomically thin MoSe<sub>2</sub>, *Nat. Commun.* 2017, 8, 1745.
- 23. Tung, I. C.; Krishnamoorthy, A.; Sadasivam, S.; Zhou, H.; Zhang, Q.; Seyler, K. L.; Clark, G.; Mannebach, E. M.; Nyby, C.; Ernst, F.; Zhu, D.; Glownia, J. M.; Kozina, M. E.; Song, S.; Nelson, S.; Kumazoe, H.; Shimojo, F.; Kalia, R. K.; Vashishta, P.; Darancet, P.; Heinz, T. F.; Nakano, A.; Xu, X.; Lindenberg, A. M.; Wen, H. Anisotropic structural dynamics of monolayer crystals revealed by femtosecond surface X-ray scattering, *Nat. Photon.* 2019, 13, 425-430.
- 24. Raman, R. K.; Murooka, Y.; Ruan, C.-Y.; Yang, T.; Berber, S.; Tománek, D. Direct observation of optically induced transient structures in graphite using ultrafast electron crystallography, *Phys. Rev. Lett.* **2008**, 101, 077401.
- 25. Harb, M.; Enquist, H.; Jurgilaitis, A.; Tuyakova, F. T.; Obraztsov, A. N.; Larsson, J. Phonon-phonon interactions in photoexcited graphite studied by ultrafast electron diffraction, *Phys. Rev. B* **2016**, 93, 104104.
- 26. Tewary, V. K.; Yang, B. Singular behavior of the Debye-Waller factor of graphene, *Phys. Rev. B* **2009**, 79, 125416.
- 27. Politano, A.; Borca, B.; Minniti, M.; Hinarejos, J. J.; Vázquez de Parga, A. L.; Farías, D.; Miranda, R. Helium reflectivity and Debye temperature of graphene grown epitaxially on Ru(0001), *Phys. Rev. B* **2011**, 84, 035450.
- 28. Schönfeld, B.; Huang, J. J.; Moss, S. C. Anisotropic mean-square displacements (MSD) in

- single crystals of 2H- and 3R-MoS<sub>2</sub>, Acta Cryst. 1983, B39, 404-407.
- 29. Skelton, E. F.; Katz, J. L. Examination of the thermal variation of the mean square atomic displacements in zinc and evaluation of the associated Debye temperature, *Phys. Rev.* **1968**, 171, 801-808.
- 30. Wang, Y. T.; Luo, C. W.; Yabushita, A.; Wu, K. H.; Kobayashi, T.; Chen, C. H.; Li, L. J. Ultrafast multi-level logic gates with spin-valley coupled polarization anisotropy in monolayer MoS<sub>2</sub>, *Sci. Rep.* **2015**, 5, 8289.
- 31. Wakabayashi, N.; Smith, H. G.; Nicklow, R. M. Lattice dynamics of hexagonal MoS<sub>2</sub> studied by neutron scattering, *Phys. Rev. B* **1975**, 12, 659-663.
- 32. Su, J.; Liu, Z.-t.; Feng, L.-p.; Li, N. Effect of temperature on thermal properties of monolayer MoS<sub>2</sub> sheet, *J. Alloys Compd.* **2015**, 622, 777-782.
- 33. Stoner, R. J.; Maris, H. J. Kapitza conductance and heat flow between solids at temperatures from 50 to 300 K, *Phys. Rev. B* **1993**, 48, 16373-16387.
- 34. Suryavanshi, S. V.; Gabourie, A. J.; Faramani, A. B.; Pop, E. Thermal boundary conductance of two-dimensional MoS<sub>2</sub> interfaces, *J. Appl. Phys.* **2019**, 126, 055107.
- 35. Dou, Z.; Chen, Z.; Li, N.; Yang, S.; Yu, Z.; Sun, Y.; Li, Y.; Liu, B.; Luo, Q.; Ma, T.; Liao, L.; Liu, Z.; Gao, P. Atomic mechanism of strong interactions at the graphene/sapphire interface, *Nat. Commun.* **2019**, 10, 5013.
- 36. Bennett, B. R.; Soref, R. A.; Alamo, J. A. D. Carrier-induced change in refractive index of InP, GaAs and InGaAsP, *IEEE J. Quantum Electron.* **1990**, 26, 113-122.
- 37. Liu, B.; Zhao, W.; Ding, Z.; Verzhbitskiy, I.; Li, L.; Lu, J.; Chen, J.; Eda, G.; Loh, K. P. Engineering bandgaps of monolayer MoS<sub>2</sub> and WS<sub>2</sub> on fluoropolymer substrates by electrostatically tuned many-body effects, *Adv. Mater.* **2016**, 28, 6457-6464.
- 38. Pogna, E. A. A.; Marsili, M.; De Fazio, D.; Dal Conte, S.; Manzoni, C.; Sangalli, D.; Yoon, D.; Lombardo, A.; Ferrari, A. C.; Marini, A.; Cerullo, G.; Prezzi, D. Photo-induced bandgap renormalization governs the ultrafast response of single-layer MoS<sub>2</sub>, *ACS Nano* **2016**, 10, 1182-1188.
- 39. Liu, F.; Ziffer, M. E.; Hansen, K. R.; Wang, J.; Zhu, X. Direct determination of band-gap

- renormalization in the photoexcited monolayer MoS<sub>2</sub>, Phys. Rev. Lett. **2019**, 122, 246803.
- 40. Docherty, C. J.; Parkinson, P.; Joyce, H. J.; Chiu, M.-H.; Chen, C.-H.; Lee, M.-Y.; Li, L.-J.; Herz, L. M.; Johnston, M. B. Ultrafast transient terahertz conductivity of monolayer MoS<sub>2</sub> and WSe<sub>2</sub> grown by chemical vapor deposition, *ACS Nano* **2014**, 8, 11147-11153.
- 41. Moody, G.; Schaibley, J.; Xu, X. Exciton dynamics in monolayer transition metal dichalcogenides, *J. Opt. Soc. Am. B* **2016**, 33, C39-C49.
- 42. Nie, Z.; Long, R.; Sun, L.; Huang, C.-C.; Zhang, J.; Xiong, Q.; Hewak, D. W.; Shen, Z.; Prezhdo, O. V.; Loh, Z.-H. Ultrafast carrier thermalization and cooling dynamics in few-layer MoS<sub>2</sub>, *ACS Nano* **2014**, 8, 10931-10940.
- 43. Wang, Q.; Ge, S.; Li, X.; Qiu, J.; Ji, Y.; Feng, J.; Sun, D. Valley carrier dynamics in monolayer molybdenum disulfide from helicity-resolved ultrafast pump–probe spectroscopy, *ACS Nano* **2013**, 7, 11087-11093.
- 44. Radisavljevic, B.; Kis, A. Mobility engineering and a metal–insulator transition in monolayer MoS<sub>2</sub>, *Nat. Mater.* **2013**, 12, 815-820.
- 45. Trucano, P.; Chen, R. Structure of graphite by neutron diffraction, *Nature* **1975**, 258, 136-137.
- 46. Chien, F. Z.; Chen, Y. S.; Chu, Y. C.; You, W. Y.; Lee, J. B.; Dann, T. E.; Tu, C. H. An X-ray measurement of Debye Waller factors of single crystal MoSe<sub>2</sub> and WSe<sub>2</sub>, *Chin. J. Phys.* **1988**, 26, 119-125.
- 47. Allen, C. S.; Liberti, E.; Kim, J. S.; Xu, Q.; Fan, Y.; He, K.; Robertson, A. W.; Zandbergen, H. W.; Warner, J. H.; Kirkland, A. I. Temperature dependence of atomic vibrations in monolayer graphene, *J. Appl. Phys.* **2015**, 118, 074302.
- 48. Chatelain, R. P.; Morrison, V. R.; Klarenaar, B. L. M.; Siwick, B. J. Coherent and incoherent electron-phonon coupling in graphite observed with radio-frequency compressed ultrafast electron diffraction, *Phys. Rev. Lett.* **2014**, 113, 235502.
- 49. Gunst, T.; Markussen, T.; Stokbro, K.; Brandbyge, M. First-principles method for electron-phonon coupling and electron mobility: applications to two-dimensional materials, *Phys. Rev. B* **2016**, 93, 035414.

- 50. Jeong, T. Y.; Jin, B. M.; Rhim, S. H.; Debbichi, L.; Park, J.; Jang, Y. D.; Lee, H. R.; Chae, D.-H.; Lee, D.; Kim, Y.-H.; Jung, S.; Yee, K. J. Coherent lattice vibrations in mono- and few-layer WSe<sub>2</sub>, *ACS Nano* **2016**, 10, 5560-5566.
- 51. He, X.; Punpongjareorn, N.; Wu, C.; Davydov, I. A.; Yang, D.-S. Ultrafast carrier dynamics of CdTe: surface effects, *J. Phys. Chem. C* **2016**, 120, 9350-9356.
- 52. He, X.; Punpongjareorn, N.; Liang, W.; Lin, Y.; Chen, C.; Jacobson, A. J.; Yang, D.-S. Photoinduced strain release and phase transition dynamics of solid-supported ultrathin vanadium dioxide, *Sci. Rep.* **2017**, 7, 10045.